Collective Bursting in Populations of Intrinsically Nonbursting Neurons

Daniel A. Blank and Ruedi Stoop

Institute of Neuroinformatics, Eidgenössische Technische Hochschule / Universität Zürich, Winterthurerstr. 190, 8057 Zürich, Switzerland

Reprint requests to PD Dr. R. S.; E-mail: ruedi@ini.phys.ethz.ch

Z. Naturforsch. **54 a,** 617–627 (1999); received September 17, 1999

We describe a novel type of bursting that we observe in simulations of large recurrent networks of biophysically plausible, intrinsically non-bursting neurons. The mechanism responsible for the bursting is a combination of excitatory feedback received from neighbouring neurons, together with an activity-dependent adaptation mechanism that slows down spiking. During the bursting phases, the firing patterns are not repeated and the lengths of the interburst intervals are varying. We develop a simple phenomenological model that captures most qualitative aspects of the observed collective bursting. We compare the parameter range leading to bursting in the phenomenological model, with parameter estimates from cortical anatomy and physiology, and conjecture that the discovered new type of bursting should also be observable in biological neocortical networks.

Key words: Bursting; Recurrent Excitation; Network Dynamics.

Introduction

Bursting is a periodic clustering of neuron discharges, separated by quiescent phases. This behaviour is observed in many different neurons, for example in neocortex, where the large pyramidal neurons in layer V typically respond with bursting discharge patterns when stimulated with current injected by an intracellular microelectrode [1, 2]. In these experiments, the current is held constant and the neurons develop the bursting autonomously (*intrinsic* bursting). The mechanisms underlying bursting have been theoretically studied, e. g., by Rinzel and Ermentrout [3], Bush and Douglas [4], Wang and Rinzel [5] and Guckenheimer *et al.* [6]. In general, to produce bursting, a mechanism is needed that includes two processes acting on different time scales: a fast process for the generation of a single action potential, and a slower process that provides the switching between repetitive spiking and quiet phases. Wang and Rinzel [5] have introduced a classification into different types of bursting depending on the behaviour of the fast and of the slow dynamics.

In our study, we will show how bursting can arise in networks of neocortical, intrinsically non-bursting neurons, where the bursting is an effect of the recurrent excitatory network architecture [7 - 10]. Bursting in recurrent networks has previously been investigated by Bush and Douglas [4]. In contrast to their approach, our neurons are not intrinsically bursting and we use no inhibitory neurons. The collective origin of our bursting leads to irregularities in the temporal structure of the bursting phases and of the quiescent phases between the bursts, even in the absence of noise (Figure 1). Both irregularities are of a stochastic nature and not chaotic (see [11]). They

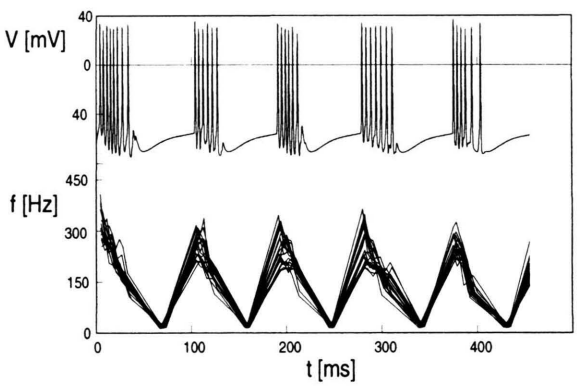

Fig. 1. Irregular spike timing in collective bursting (network simulation). *Top:* Development of the membrane voltage of one neuron out of a population of 20 neurons. *Bottom:* Instantaneous firing rates have been calculated as follows: Points with abscissa = center of the interspike interval (ISI), ordinate = inverse of the ISI size, are connected, for each of the 20 neurons of the network.

0932–0784 / 99 / 1000–0617 $ 06.00

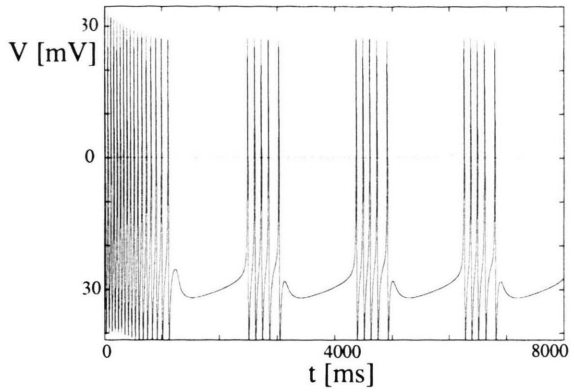

Fig. 2. When slow positive and negative feedback is added to the Morris-Lecar model, regular bursting emerges, after an initial build-up phase.

are expected to decrease with the number of neurons in the network [12]. This differs from the behaviour of intrinsically bursting neurons, which show regular spiking patterns during the bursting phase, and it differs from the irregular bursting observed by Bush and Douglas [4], which they claim to be chaotic. Furthermore, the type of bursting that we describe here does not fit into the classification by Wang and Rinzel [5], but is a new phenomenon.

We will first review the principles that are followed by single, intrinsically bursting neurons. Then we describe our new collective bursting, that we observed in simulations of biophysically plausible neuronal networks. The high-dimensional neural network behaviour will be approximated by a series of refined phenomenological models, until its most prominent qualitative features are matched. The parameters of the simplified model can then be compared to estimates from physiology and anatomy of the neocortex, from where we draw conclusions on the observability of this new bursting type in *in vivo* neocortical networks.

Intrinsically Bursting Neurons

A fundamental model of a bursting neuron is the modified [3, 6] Morris-Lecar model [13]. It consists of two fast processes that generate the repetitive spiking: a fast, voltage-gated calcium current for the depolarization of the membrane potential and a delayed rectifier potassium current for repolarization. To generate bursting, two additional slow currents are essential: a slow calcium-dependent potassium current and a calcium current with slow dynamics and low voltage threshold. The slow potassium current provides a negative feedback that leads to an adaptation of the firing rate and eventually stops the firing. The slow calcium current provides a positive feedback by causing a depolarization of the membrane, and thereby restarting the firing activity. The interaction of these two mechanisms generates bursts of spikes that ride on the positive feedback-dominated part of the neuron dynamics. An example of an intrinsically bursting neuron from the modified Morris-Lecar model [3] is shown in Figure 2. The corresponding parameters are given in the Appendix. Note the perfect regularity of the bursting after an initial build-up phase. The spiking pattern is the same for every burst.

An unsatisfactory shortcoming of this model, if compared to real neurons, is that it is geometrically a point model. As can be expected, the introduction of spatial structures with distributed ion channels introduces an additional degree of complexity. Mainen and Sejnowski [14] investigated the influence of dendritic morphology on the discharge pattern of the neuron. They constructed a model with two compartments, representing soma and dendrite. Again, the behaviour of the model is determined by the different kinetics of the voltage-gated conductances of the ionic currents. A very fast sodium conductance, strong in the soma and weaker in the dendrite, generates a depolarization of the membrane upon stimulation. A fast potassium conductance in the soma repolarizes the membrane after spiking. Slow potassium channels in the soma and in the dendrite provide an extended after-spike hyperpolarization, that is able to shut off bursting. A slow calcium conductance finally generates a positive feedback current in the dendrite and re-enables bursting. Depending on the degree of the coupling between the fast conductances in the soma and the slower conductances in the dendrite, the model produces a variety of different firing patterns for fixed values of the conductances. Figure 3 shows a typical bursting pattern that is observed in this model. In this figure, the (negative) current flow from the dendrite to the soma evidences how the dendritic conductances provide additional current after the somatic conductances have triggered the spike. Characteristically, the first spike in a burst has a bigger amplitude than successive spikes. This is, because the somatic conductances are partly inactivated after the first spike at the time when the dendritic currents arrive. The bursting pattern becomes regular after a transient phase,

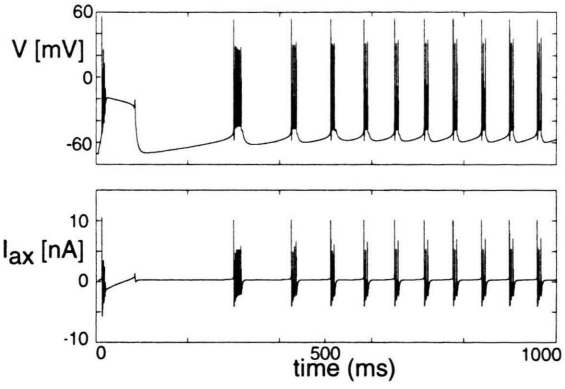

Fig. 3. Bursting from the Mainen-Sejnowski model, which takes into account the spatial extension of the neuron. *Top:* Membrane voltage showing identical bursting after an initial build-up phase. The first spike in a burst has the largest amplitude, which is due to the inactivation of the somatic ion channels after the first spike. The regularity of the bursting is preserved. *Bottom:* Axial current between somatic and dendritic compartment. A positive current indicates current flow from soma to dendrite. During a burst, the dendrite generates new charge which flows towards the soma.

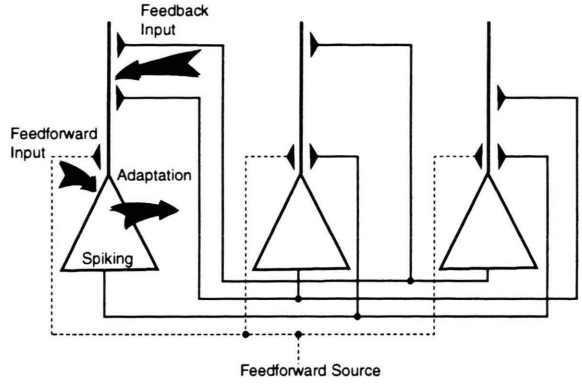

Fig. 4. Principle of recurrently connected neurons, receiving both feedforward and feedback input current. The synaptic currents flow into the dendrite and contribute to spiking, while the adaptation current in the soma flows out of the cell and inhibits spiking.

similar to the behaviour of the bursting Morris-Lecar model. However, the Mainen-Sejnowski model is able to generate more complex discharge patterns (see [14] for illustrations). This is not only due to the increased number of more complex currents, but also an effect of the separation into two compartments, i. e. of the nonuniformity of the membrane voltage.

Collective Bursting from Nonbursting Neurons

Let us now outline how bursting arises in networks of recurrently connected, biophysically plausible model neurons that are *not* intrinsically bursting. Our modeling paradigm is an abstraction of the way spiny stellate neurons are embedded in layer IV of the neocortical network. Spiny stellate neurons receive *feedforward* input from the thalamus and they are strongly connected among themselves by excitatory synapses. Accordingly, in our model spiny stellate neurons are connected in the all-to-all way, and each neuron receives feedforward input from outside of the network (see Figure 4). In the *Appendix*, we give a detailed description of the biophysically plausible models of spiny stellate neurons from cat striate cortex. Analogous to single-cell bursting, processes that occur on different time scales are responsible for the emergence of bursting. The fast time scale is given by the fast kinetics of the sodium and potassium currents that generate a single spike. The slower time scale is given by the feedback excitation from the recurrently connected neighbours, which arrives with a delay of roughly one interspike interval. This is the time it takes for a change in the feedforward input to modify the firing rate. An additional, much slower negative adaptation feedback is responsible for slowing down the firing activity (see Figure 4).

Upon the arrival of the independent external input, the neurons in the network start to fire. The recurrent excitation quickly builds up and causes the cells to fire at even increased firing rates, due to the positive feedback. The spiking then activates the adaptation mechanism: a voltage-dependent calcium current sets in and causes the intracellular calcium concentration to rise. This triggers a calcium-dependent potassium current that hyperpolarizes the membrane voltage, which terminates the burst of spikes. When the calcium concentration has decayed due to intracellular diffusion and buffering, the cell becomes ready for another burst, and the cycle starts again. Similar to the bursting Morris-Lecar model, the adaptation mechanism acts as a negative feedback. However, the source of the positive feedback is no longer intrinsic to a single neuron, but is produced by the concurrently active neurons in the population. The nature of this collective feedback is quite different to the one of an intrinsic burster: it is produced by the sum of isolated synaptic events, scattered over time. In a recent study, Crook *et al.* [15] investigated the influence of spike rate adaptation on the synchronization properties of

weakly connected neurons. They found that adaptation enhances synchronous spiking with zero phase lag. Bursting is not observed in their model because of the weakness of their excitatory feedback. Their study also differs from the present one because the parameters of our model neurons are varied across the population, to account for the large variability of neuron responses *in vivo*. As a consequence, individual neurons in our network respond with a spread of discharge rates to identical amounts of current. In addition, our simulation takes care of variable delay of interaction times and of varying interaction strengths.

The variability between the neurons in our simulation causes them to burst only in an approximately synchronized manner. Moreover, as all interspike intervals are governed by the neuron's individual current-discharge relationship, the lengths of the interburst intervals are varying from neuron to neuron. However, the strong excitatory coupling causes collective bursts, with individual variations of onset usually within one burst interspike interval.

Population Models of Collective Bursting

To be able to compare the conditions for bursting in our network simulations with natural neocortical network conditions, we will evolve a line of phenomenological models that are finally able to qualitatively reproduce the results of our network simulations.

As all neurons in the network are assumed to behave in a similar way, it is tempting to model the population by a single representative neuron. The firing activity of this "population" neuron would be described by the relation

$$f = h(I_{\mathrm{ff}} + I_{\mathrm{fb}} - A), \tag{1}$$

where f stands for the firing frequency as a function of the total input currents summated at the soma. Synaptic feedforward current I_{ff} (from an external source) and feedback current I_{fb} (from recurrent excitation) contribute to an increase in firing rate; the firing rate is reduced by the adaptation current A. The sum of currents is related to the firing rate by an activation function h, for which we will use different forms of increasing complexity, to approach the bursting properties observed in the network simulations. A similar modeling approach was used by Douglas *et al.* [10, 16], which, however, was based on a different network structure and where the role of the activation function remained unexplored.

The dynamics of A and I_{fb} are given by the set of relations

$$A_\infty(f) := \mu f, \tag{2}$$

$$I_{\mathrm{fb}\infty}(f) := \alpha f, \tag{3}$$

$$\frac{\mathrm{d}A}{\mathrm{d}t} = \frac{A_\infty - A}{\tau_{\mathrm{A}}} = \frac{\mu f - A}{\tau_{\mathrm{A}}} = \frac{\mu h(I_{\mathrm{ff}} + I_{\mathrm{fb}} - A) - A}{\tau_{\mathrm{A}}}, \tag{4}$$

$$\frac{\mathrm{d}I_{\mathrm{fb}}}{\mathrm{d}t} = \frac{I_{\mathrm{fb}\infty} - I_{\mathrm{fb}}}{\tau_{\mathrm{fb}}} = \frac{\alpha f - I_{\mathrm{fb}}}{\tau_{\mathrm{fb}}} = \frac{\alpha h(I_{\mathrm{ff}} + I_{\mathrm{fb}} - A) - I_{\mathrm{fb}}}{\tau_{\mathrm{fb}}}, \tag{5}$$

where μ is the neuron's constant of adaptation and α is the network feedback constant. τ_{A} and τ_{fb} are the time constants of the adaptation and of the network feedback, respectively. Unless stated otherwise, we always use the parameter values given in Table 2 of the Appendix. We first discuss the collective properties that can be obtained by choosing the simplest nontrivial activation function. In this case, h has a linear dependence on the input current:

$$h(I) = GI, \tag{6}$$

where G denotes an effective "spike" conductance [10]. Using the rescaling

$$T = t/\tau_{\mathrm{A}},$$
$$M = \mu G,$$
$$K = \alpha G,$$
$$\tau = \tau_{\mathrm{fb}}/\tau_{\mathrm{A}},$$

we arrive at the equation

$$\frac{\mathrm{d}A}{\mathrm{d}T} = M(I_{\mathrm{ff}} + I_{\mathrm{fb}} - A) - A, \tag{7}$$

$$\frac{\mathrm{d}I_{\mathrm{fb}}}{\mathrm{d}T} = \frac{K(I_{\mathrm{ff}} + I_{\mathrm{fb}} - A) - I_{\mathrm{fb}}}{\tau}, \tag{8}$$

which describes the system in terms of the dimensionless parameters M, K and τ. As this differential

equation is linear and two-dimensional, the eigenvalues of the Jacobian matrix

$$\boldsymbol{J} = \begin{pmatrix} -(M+1) & M \\ -K/\tau_{\mathrm{fb}} & (K-1)/\tau_{\mathrm{fb}} \end{pmatrix}$$

fully describe the time evolution. Chaos is prohibited, and oscillations are only possible in the special case of a vanishing trace of the Jacobian [17]:

$$-(M+1) + \frac{K-1}{\tau_{\mathrm{fb}}} = 0. \tag{9}$$

For parameters such that the trace of matrix $\boldsymbol{J}$ is negative, the system will therefore spiral in to a fixed-point, with

$$A = A_\infty, \tag{10}$$
$$I_{\mathrm{fb}} = I_{\mathrm{fb}\infty}, \tag{11}$$

and from (2) - (5), we obtain for this case the analytical solution

$$A_\infty = -\frac{I_{\mathrm{ff}} M}{K - M - 1},$$
$$I_{\mathrm{fb}\infty} = -\frac{I_{\mathrm{ff}} K}{K - M - 1}.$$

The discharge rate of the associated steady state can be evaluated using (1). It demonstrates the inadequateness of this model: even at positive parameters, the instantaneous firing rates may temporarily become negative! This happens for parameter values that lead to very small traces of $\boldsymbol{J}$, when the system exhibits a damped oscillation towards the fixed point. For positive traces of $\boldsymbol{J}$, the spiral will become unstable; the firing rates "explode", i.e., they will grow infinitely with time.

Negative instantaneous firing rates are excluded if a threshold is introduced in the activation function. In the simplest case, this leads to the linear-threshold model, as used in the study of Douglas *et al.* [10]:

$$h_{\mathrm{l}}(I) = G \cdot \mathrm{thresh}(I, I_{\mathrm{th}}),$$

where

$$\mathrm{thresh}(I, I_{\mathrm{th}}) = \begin{cases} 0 & \text{for } I < I_{th}, \\ I - I_{\mathrm{th}} & \text{for } I \geq I_{\mathrm{th}}. \end{cases}$$

For this activation function, net currents below the threshold current I_{th} will not produce spiking. The nonlinearity introduced by the threshold leads to a much richer behaviour of the system. As a function of the recurrent feedback parameter K, a (subcritical) Hopf bifurcation emerges and oscillations of A (and therefore of f) are observed (see Figure 5). In terms of the population model, this implies that bursting behaviour is observed for values of the recurrent coupling strength K beyond the critical value (see Figure 6). When this value is crossed, there is no

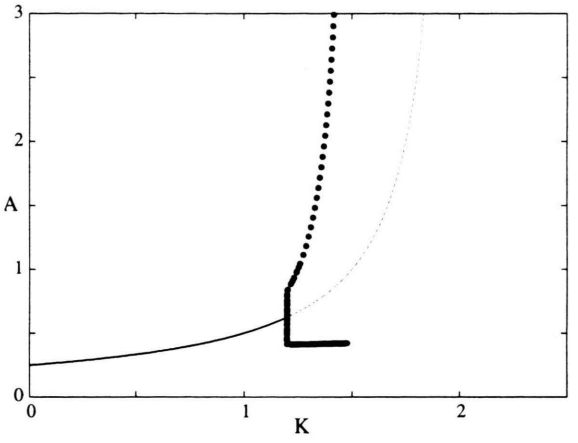

Fig. 5. Varying the recurrent coupling K in the linear threshold model leads to a Hopf bifurcation at $K = 1.2$ and oscillatory solutions (filled circles). Due to the hard onset of the bifurcation, only oscillatons with nonzero amplitude are possible, where the oscillation amplidude grows exponentially with K. For K greater than 2, the firing rates diverge for any nonzero feedforward current.

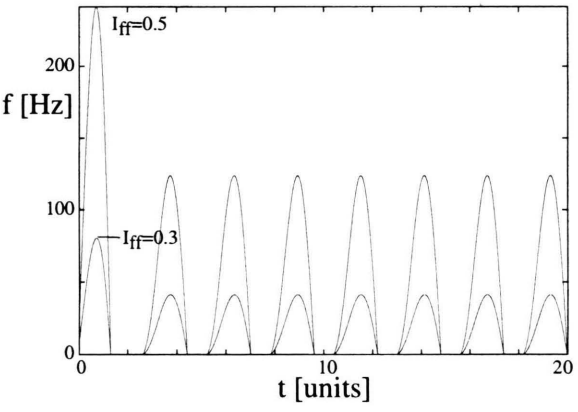

Fig. 6. Oscillations of the instantaneous firing rate f in response to feedforward currents of 0.3 (*bottom*) and 0.5 nA (*top*), respectively. The frequency of the bursts is independent of the stimulus strength I_{ff} (linear threshold model).

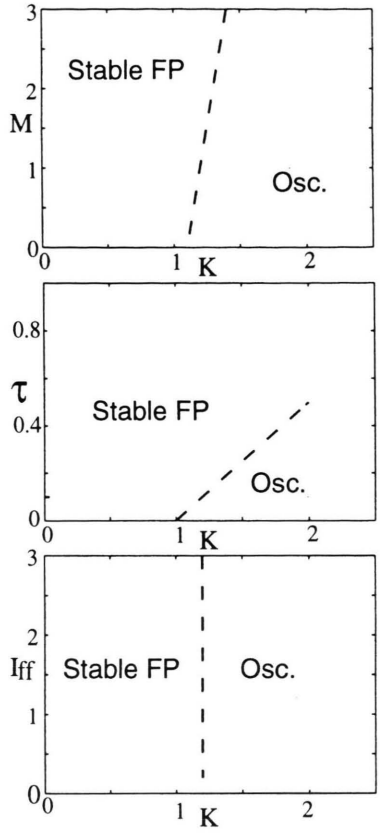

Fig. 7. Dependence of the bifurcation from stable fixed points to oscillations, on the main system parameters. The dashed lines separate stable fixed point from stable oscillation behaviour. *Bottom:* The Hopf bifurcation is independent of the strength of the feedforward current I_{ff} (linear threshold model).

graded onset of bursting. Instead the firing rate jumps immediately.

It is of interest to explore the dependence of the oscillations on other model parameters. For this purpose, we follow the bifurcation points in the $M - K$ and $\tau - K$ planes. Bursting is possible when K exceeds a critical value $K_{\mathrm{c}}(M)$ or $K_{\mathrm{c}}(\tau)$, respectively (see the thick dashed lines in Figure 7. Figure 8 shows how the oscillation amplitudes depend on τ: they diverge when the value of approximately $\tau_{\mathrm{c}} = 0.07$ (dimensionless units) is approached. The biophysical interpretation of this fact is, that the feedback dominates the system behaviour, because it arrives before the adaptation has a chance to become effective. In contrast, the bifurcation behaviour is independent of the feedforward current I_{ff} (see bottom panel of Fig. 7) and of the threshold current I_{th} (not shown).

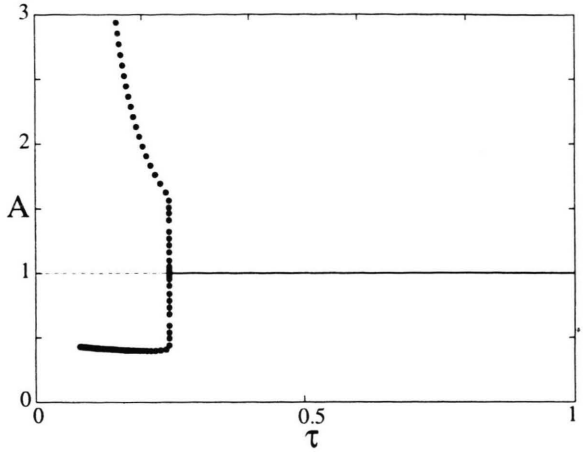

Fig. 8. Bifurcation diagram for variable τ, for $K = 1.5$. As could be expected from the middle panel of Fig. 7, the subcritical Hopf bifurcation occurs at $\tau = 0.25$. The oscillation amplitude grows infinitely as τ approaches $\tau_{\mathrm{c}} = 0.07$ from above (linear threshold model).

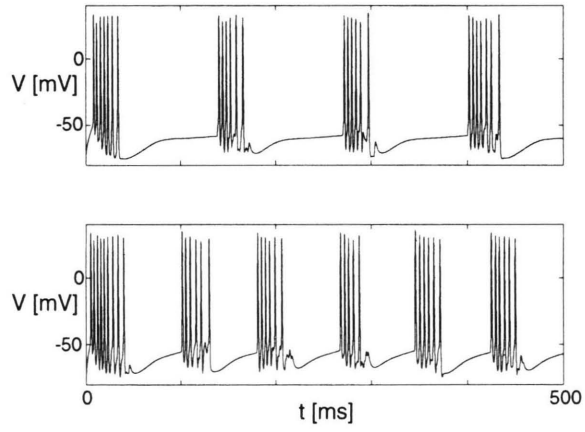

Fig. 9. Voltage traces of a representative neuron in the biophysical network simulation. *Top:* Bursting discharge pattern in response to an injected feedforward current of 0.3 nA. *Bottom:* Discharge for 0.5 nA. Note how the frequency of the bursts increases for stronger feedforward current.

Increasing the feedforward current I_{ff} increases the amplitude of the discharge-rate oscillation. However, it does not affect the phases at which the oscillations occur (Figure 6). Networks of recurrently connected neurons that always show regular spiking behaviour can be used as perfect firing-rate amplifiers [10]: they amplify the feedforward input rate while maintaining simple discharge patterns.

We now compare the behaviour of this phenomenological population model with the behaviour of the

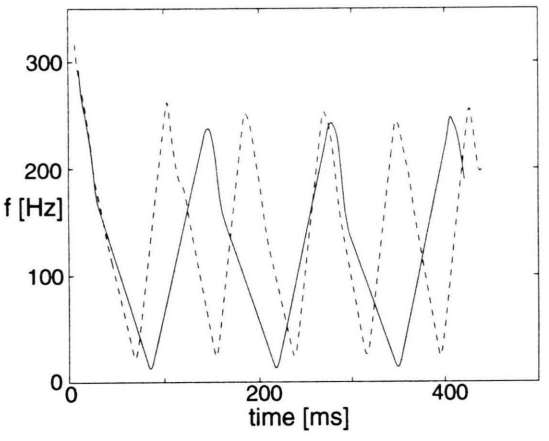

Fig. 10. Instantaneous firing rates for the spike trains in Fig. 9 (*Solid line:* 0.3 nA. *Dashed line:* 0.5 nA). Instantaneous rates are the inverse of the interspike intervals and are thus plotted in the middle of the intervals. The peak burst rate is relatively constant for the two injection strenghts, suggesting that the discharge rate of the modeled neuron is saturating for strong currents.

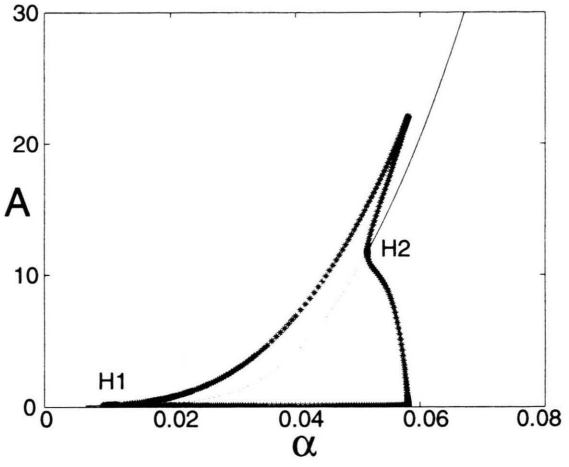

Fig. 11. Two Hopf bifurcations are occuring for the power function threshold model. Increasing the recurrent coupling α leads from steady-state solutions (*solid line*), to oscillating, bursting behaviour at $\alpha = 0.0095$ (*filled circles*) and again to steady solutions for $\alpha = 0.052$ and stronger coupling.

biophysically motivated network simulation. In a simulation comprising only 20 spiking neurons, highly variable bursting is apparent for feedforward currents of 0.3 and 0.5 nA, see Figure 9. In contrast to the phenomenological model, the network simulation shows a marked increase of the frequency of the bursts for increased firing rates. At moderately strong feedforward currents the interburst intervals are shortened while the burst firing rates remain relatively constant (see Figure 10). At very large input currents, due to the continued shortening of the quiescent phases, the system returns to regular spiking. Constant firing rates during a burst indicate a saturation of the firing rate as a function of the current. The saturation is most prominent during the bursting period, since this is when the neuron receives maximal excitatory current from recurrent synapses and from voltage-dependent channels.

As the final step in our modeling approach, we aim at including this saturation in our phenomenological model. We found that the observed saturation phenomenon can be modeled by a power function threshold model:

$$h_{\mathrm{p}}(I) = u \cdot \mathrm{thresh}(I, I_{\mathrm{th}}, v), \tag{12}$$

with

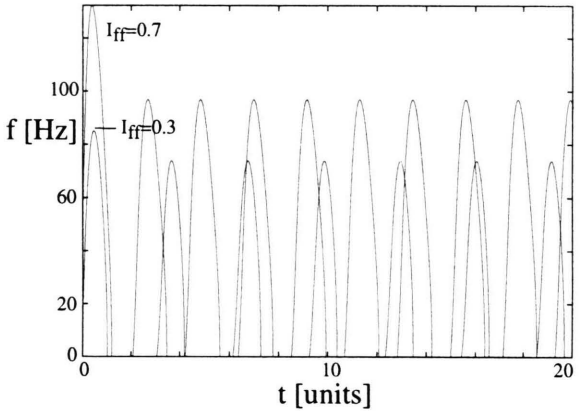

Fig. 12. For the power function threshold model, an increase of the burst frequency emerges for stronger currents, as observed in the network simulation (Figure 10).

$$\mathrm{thresh}(I, I_{\mathrm{th}}, v) = \begin{cases} 0 & \text{for } I < I_{\mathrm{th}}, \\ (I - I_{\mathrm{th}})^v & \text{for } I \geq I_{\mathrm{th}}, \end{cases}$$

where $u = 74.82$ and $v = 0.7043$ are phenomenological parameters, resulting from fitting $h_{\mathrm{p}}(I)$ to the f-I curve of a compartmental model.

To derive the properties of this new model, it is convenient to use the feedback parameter α instead of the nondimensionalized recurrent coupling K (where the relevant relations are $\alpha = N \cdot q$, N = Number of

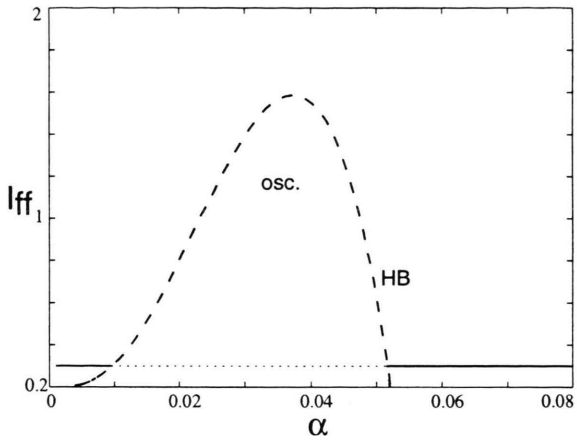

Fig. 13. Dependence of the bifurcation point on the feedforward current and on the recurrent connectivity in the power function threshold model. *Thick dashing:* Location of the Hopf bifurcation (HB). Oscillatory solutions lie below this line (osc.). The horizontal line represents the example of a feedforward current of 0.3 nA, with a firing threshold of 0.2 nA. *Full lines:* stable fixed points. *Thin dashing:* unstable fixed points.

recurrent synapses, q = recurrent current per synapse. For numbers, see *Appendix*). Figure 11 shows the bifurcation diagram for the power function threshold model as a function of the recurrent coupling α. Two Hopf bifurcations occur. The first bifurcation appears when α is increased from zero. It changes spiking at a fixed discharge rate to oscillating, bursting behaviour. The second (reverse) bifurcation appears when the oscillations are suppressed by strong coupling and the system returns to regular spiking. Numerical investigations show that these observations also persist in the presence of noise. The power function threshold leads to the desired increase of the burst frequency as a function of the injected current (see Figure 12). The interspike intervals – and therefore also the instantaneous discharge rates – now vary much less during the bursting phase, than in the previous model (Figure 6). This also is in better correspondence with the network simulations (Figure 10). The dependence of the model on the feedforward current I_{ff} is captured in the bifurcation diagram of Figure 13. Bursting behaviour is possible for values of I_{ff} below the dashed line. Above the bifurcation curve the oscillations are damped and settle to steady discharge rates. A similar transition from bursting to regular spiking for increased current has also been found in models of intrinsically bursting neurons of layer V [18]. The simplification that is inherent in the phenomenological power function threshold model systematically neglects the effects introduced by neurons with different morphologies and different current-discharge relationships. Therefore, even in this most elaborate phenomenological model, all bursting is regular: the interburst intervals are constant and the burst phases always show the same time courses, as was already the case in the two introductory bursting models. This is in marked contrast to the biophysically plausible network simulation, where the spike timings are irregular and where the interspike intervals are governed by each neuron's individual current-discharge relationship, and by the synaptic coupling with varying delay between the neurons.

Anatomical and Physiological Parameter Verification

To support our conjecture that the observed bursting phenomenon should be observable in abundance in biological neural networks, we perform a comparison between the simulation parameters and available physiological estimates. The nondimensionalized parameter $K = \alpha \cdot G$ is based on assumptions about the recurrent connectivity α, and on a mean slope G of the current-discharge relationship. Douglas *et al.* [10] estimate that for spiny stellate neurons, $\alpha = N \cdot q = N \cdot 0.0001$ [nA/spike/sec]. In an unpublished study, we investigate the influence of the presynaptic discharge rate on the dendritic current transfer. We find a value of $\alpha = N \cdot$ current/synapse = $N \cdot 0.0002$ nA/spike/sec (average current!), for a population discharging at 50 Hz. A value for the slope of the current-discharge relationship can be found in the study by Ahmed *et al.* [19] of deep and superficial layer pyramidal neurons. According to them, a typical cell from the deep layers may have a mean slope of roughly 100 Hz/nA, in the unadapted state. Superficial layer cells may have a mean slope of only 50 Hz/nA. Combining these two estimates, we find that for mean values of α and G, K will be in the range of one for a population size of $N = 100$, and would therefore already be close to the parameter region of oscillatory behaviour (see Fig. 7, bottom). From [19], we also obtain an estimate for the adaptation strength M. There, the authors measured the degree of adaptation in cortical neurons from different layers, and expressed it as the ratio r = (peak firing rate – adapted firing rate)/peak firing rate. Superficial layer cells seem to adapt strongly, up to 67%, while

deep layer cells adapt to 51%. The corresponding value of r from our model is obtained as follows: If current is injected only into one neuron and the rest of cortex is not stimulated, we have $I_{\mathrm{fb}} = 0$. For the fully adapted state, we obtain

$$A_\infty = M(I_{\mathrm{ff}} - A) = \frac{MI_{\mathrm{ff}}}{1+M}; \tag{13}$$

inserting this into (1) yields

$$f = G(I_{\mathrm{ff}} - \frac{MI_{\mathrm{ff}}}{1+M}) \quad = \quad GI_{\mathrm{ff}}(1 - \frac{M}{1+M}),$$

which leads to

$$r \quad = \quad \frac{GI_{\mathrm{ff}} - GI_{\mathrm{ff}}(1 - \frac{M}{1+M})}{GI_{\mathrm{ff}}} = \frac{M}{1+M}.$$

Therefore, for a value of $M = 2$, the ratio r is 66%, which is in good agreement with the experimental estimate.

The ratio of the time constant of adaptation to the time constant of the feedback τ, has a strong impact on the system behaviour. Our estimate for the feedback time constant is of the order of one interspike interval, as a spiking neuron is responding almost immediately to a change in input current (and is essentially unrelated with the membrane time constant [20]). According to Stratford *et al.* [21], synaptic latencies in local circuits are shorter than 2 ms. We can compare the feedback time in local circuits of neurons discharging at 100 Hz in the simulation, to the exponential time course of the feedback in the phenomenological model. There, the feedback rises exponentially to 98% within 4τ. In the comparison with the network simulation, this time should be equivalent to the sum of one interspike interval and the synaptic delay. Consequently, we obtain the estimate $4\tau_{\mathrm{fb}} = (10 + 2)$ ms, from which we derive $\tau_{\mathrm{fb}} \simeq 3$ ms. An estimate for τ_{A} can be obtained again from [19]. The authors find, that superficial layer cells are significantly faster adapting than deep layer cells with adaptation time constants of 11.5 compared to 51.4 ms. Hence, the corresponding nondimensional model time constant $\tau = \tau_{\mathrm{fb}}/\tau_{\mathrm{A}}$ is between 0.06 and 0.26. From the middle panel of Fig. 7, we conclude that for deep layer neurons with a nondimensional time constant of about 0.06, bursting is possible, for recurrent couplings not much greater than one. Superficial layer cells will need the much stronger coupling of approximately $K = 1.5$ to generate bursting behaviour.

Conclusions

We evolved a phenomenological model with thresholding, spike rate adaptation and saturation that is able to reproduce the collective bursting in a recurrent network of inhomogeneous, intrinsically non-bursting neurons. The observed bursting is of a novel type, as it emerges from the recurrent excitation between neurons and their adaptation of firing rates. When the network bursting is reduced to a simple model, the irregularity of spiking is lost and the bursting oscillations become regular, similar to the behaviour of models of intrinsically bursting cells [5]. The comparison of the parameter regime in which the model is bursting, with estimates from physiological experiments, suggests that real cortical networks are likely to show this bursting behaviour, especially for circuits in the deeper layers of the cortex. We have seen that the dynamic range of the burst discharge rates is limited by the saturation of the current-discharge curves for strong net currents, both in our power function threshold model and in the network simulation. In *in vivo* experiments, commonly the interspike interval distributions are measured. In the presence of the described bursting, we expect clusters around a short interval that corresponds to the high discharge rates during the burst. This interval will be insensitive towards input current changes. A second cluster will be formed by the interburst intervals. Because biological neurons respond to increased input currents by a shortening of the interburst intervals, this cluster will be sensitive towards changes of the input current.

Our discovery implies that the identification of bursts *in vivo* should include the possibility of intrinsically non-bursting network bursters. While it may be impossible to distinguish the two types of bursters from the interspike interval distributions, a current injection into a single neuron will allow for such a distinction. About the function of the bursts, we can only speculate. Chagnac-Amitai and Connors [22] have proposed that intrinsically bursting neurons tend to drive synchronized excitation and inhibition in cortex. In our case, the collective activity drives all coupled neurons to bursting almost simultaneously, with the precise onset of bursting scattered over not more than one interspike interval (Figure 1).

In this respect, the collective bursting may be seen as a coarse-scale synchronized excitation. Whether this type of synchronized activity plays an essential role in the context of coding by synchronization, remains still to be explored. The role of inhibition has not been included in our study but we expect that recurrent inhibition will also be synchronized [23]. It is clear that our studied excitatory network does not occur in this pure form in the cortex. However, it provides an explicit minimal model for the generation of collective bursting in recurrent networks.

Appendix: Methods

Network Simulations

Our biophysically plausible network simulations are based on simplified compartmental neurons. These model neurons were derived from a reconstructed cat spiny stellate neuron from layer 4 of the striate cortex, where we used the algorithm of Bush and Sejnowski [24] to simplify the detailed reconstructed geometry of the cell into an 8-compartment version. Compartment geometries were varied randomly (±10%), to account for the variability seen in biological neurons. Each cell was equipped with somatic voltage-dependent conductances, as follows:

- fast sodium and potassium conductances for the generation of an action potential,
- an A-type potassium conductance that linearizes the f-I curve in the perithreshold region,
- a high-voltage-activated calcium and a calcium-dependent potassium conductance for an adaptation of discharge.

The conductance models are described in Bernander *et al.* [25] and Bernander [26]. Detailed conductance parameters are given in Table 1; they are adopted from [26].

The numerical simulations were performed with the use of the NEURON simulation environment [27]. The chosen passive properties were R_m = 5'000 [Ω cm^2] and C_m = 2 μF/cm^2. With inserted active conductances, the input resistance of the simplified model was 88 MΩ, at resting membrane potential. Synapses were modeled by a current injection into the somatic compartment, with a current function $I_{syn}(t) = \bar{g} \cdot E_{dr} \cdot (t/\tau_{syn}) \exp(1 - t/\tau_{syn})$, where τ_{syn} = 0.5 ms. The driving force was fixed to E_{dr} = –40 mV, to prevent an unrealistic sublinear summation of synaptic inputs in the simplified cell model. The synaptic peak conductances and latencies were varied using Gaussian distributions, with *mean* = 0.007 and standard deviation σ = 0.00084 mS for the conductance, and *mean* = 1.7 and σ = 0.7 ms for the delay. The variations of the neuron geometries account for the variability of the current-discharge relationships observed in *in vivo* experiments [19].

Table 1. Parameters for the compartmental simulation.

$\bar{g}_{Na}$	0.12 S/cm^2
$\bar{g}_{K\,fast}$	0.07 S/cm^2
$\bar{g}_{Ca}$	0.0005 S/cm^2
$\bar{g}_{K_{Ca}}$	0.04 S/cm^2
$\bar{g}_{KA}$	0.001 S/cm^2

Table 2. Simulation parameters (dimensionless).

α	0.01
$\tau = \tau_{fb}/\tau_A$	0.1
μ	0.02
I_{th}	0.2

Phenomenological Models

Table 2 lists the parameters that are used in our phenomenological models.

The figures of the phenomenological models were generated with the help of the program package XPP.

Acknowledgements

This research was supported by the Swiss National Foundation 5002-42787 and by a KTI grant (with Phonak AG). We would like to thank J. C. Anderson, R. J. Douglas and K. A. C. Martin for providing us with the spiny stellate morphology.

[1] B. W. Connors and M. J. Gutnick, Trends Neurosci. **13**, 99 (1990).
[2] A. Mason and L. Larkman, J. Neurosci. **10**, 1415 (1990).
[3] J. Rinzel, and B. Ermentrout, Methods of Neural Modeling: From Synapses to Networks; Chapt.: Analysis of neural excitability and oscillations, MIT Press 1989.
[4] P. C. Bush, and R. J. Douglas, Neural. Comput. **3**, 19 (1991).
[5] X. J. Wang and J. Rinzel, The Handbook of Brain Theory and Neural Networks; Chapt.: Oscillatory and bursting properties of neurons, MIT Press 1995.
[6] J. Guckenheimer, R. Harris-Warrick, J. Peck, and A. Willms, J. Comput. Neurosci. **4**, 257 (1997).
[7] R. Lorente de Nó, J. Neuronphysiol. **1**, 207 (1938).
[8] R. J. Douglas, K. A. C. Martin, and D. Whitteridge, Neural Comput. **1**, 480 (1991).
[9] C. M. Gray, J. Comput. Neurosci. **1**, 11 (1994).
[10] R. J. Douglas, C. Koch, M. A. Mahowald, K. A. C. Martin, and H. Suarez, Science **269**, 981 (1995).
[11] J. Peinke, J. Parisi, O. E. Roessler, and R. Stoop, Encounter with Chaos, Springer-Verlag, Berlin 1992.
[12] Note, however, that the existence of a "thermodynamic" limit for our system is highly questionable.
[13] C. Morris and H. Lecar, Biophys. J. **35**, 193 (1981).
[14] Z. F. Mainen and T. J. Sejnowski, Nature London **382** (6589), 363 (1996).
[15] S. M. Crook, G. B. Ermentrout, and J. M. Bower, Neural. Comput. **10**, 837 (1998).
[16] R. J. Douglas, C. Koch, M. Mahowald, and K. A. C. Martin, Cerebral Cortex, Vol. 13, Chapt.: The role of recurrent excitation in neocortical circuits, Kluwer Academic / Plenum Publishers, 1999, ps. 251-82.
[17] S. H. Strogatz, Nonlinear dynamics and chaos: with applications to physics, biology, chemistry and engineering, Addison-Wesley, 1994.
[18] P. A. Rhodes and C. M. Gray, Neural Comput. **6**, 1086 (1994).
[19] B. Ahmed, J. C. Anderson, R. J. Douglas, K. A. Martin, and D. Whitteridge, Cereb. Cortex **8**, 462 (1998).
[20] C. Koch, M. Rapp, and I. Segev, Cereb. Cortex **6**, 93 (1996).
[21] K. J. Stratford, K. Tarczy-Hornoch, K. A. C. Martin, N. J. Bannister, and J. J. B. Jack, Nature London **382**, 258 (1996).
[22] Y. Chagnac-Amitai and B. W. Connors, J. Neurophysiol. **62**, 1149 (1989).
[23] R. Stoop, K. Schindler, and L. A. Bunimovich, Phys. Lett. A **258**, 115 (1999).
[24] P. C. Bush, and T. J. Sejnowski, J. Neurosci. Meth. **46**, 149 (1993).
[25] Ö. Bernander, R. J. Douglas, K. A. C. Martin, and C. Koch, Proc. Natl. Acad. Sci. USA **88**, 11569 (1991).
[26] Ö. Bernander, Synaptic Integration and its control in neocortical pyramidal cells. PhD thesis, California Institute of Technology, 1993.
[27] M. Hines, Int. J. Biomed. Comput. **24**, 55 (1989).